Rocky Worlds DDT: JWST Data Analysis Report for GJ 3929 b

Joshua D. Lothringer, Elena Manjavacas, and Taylor J. Bell
JWST Data Analysis Team

April 02, 2026

1 Observation Overview

Under the RWDDT program, JWST-DDT-9235 Observations 4 and 5 obtained time-series imaging of the fourth eclipse of GJ 3929 b using MIRI/F1500W with the SUB128 subarray, covering a total of 7.33 hours with the goal of measuring the secondary eclipse of the planet. The long duration of this observation required the observation to be split into two exposures or two visits due to the total number of frames exceeding the 196 608 maximum.

In an attempt to schedule the change between exposures/visits, the observation was broken into two visits of unequal length with the break (and corresponding ∼15-minute pause in integrations) scheduled to occur before the median circular-orbit eclipse time and after the median eccentric-orbit eclipse time as estimated by the RWDDT Core Implementation Team's JWST Scheduling Sub-Team before any of the JWST eclipse observations of GJ 3929 b were collected.

The analysis presented here uses data only from Observations 4 and 5. Given the poor constraints on the planet's orbital eccentricity and the low expected signal-to-noise ratio of the eclipse signal, we expect at most a marginal detection of the eclipse from this observation alone. Future analyses incorporating all RWDDT visits and additional datasets may yield a more robust detection of planet's eclipse.

2 Data Reduction

This report presents results from two reductions and analyses performed by Analyst A (Lothringer) and Analyst B (Manjavacas). Both analyses used the standard JWST pipeline (v1.20.2 with CRDS context `jwst1464.pmap`) for detector-level calibrations. Stage 1 processing included running the following steps: Stage 1 processing included running the following steps: `emicorr`, `saturation`, `firstframe`, `lastframe`, `reset`, `linearity`, `rscd`, `dark current` and `jump` (with the threshold increased from 4.0 to 8.0). In Stage 2 we ran the `flat_field` step, but we disabled the `photom` step as flux-calibrated data are not desired for time-series analyses.

Next, we used `Eureka!` (version 1.4.dev106+g3a6724481) to extract the photometric time-series (Stage 3), identify and correct for any outliers (Stage 4), and then fit a systematics and transit model to the time-series (Stage 5). A time-series was constructed for each pixel in Stage 3, and any outlier exceeding 5σ (along with any `NaN` value) was replaced with a bi-linear interpolation using its nearest neighbors. Next, a center-of-mass centroid was calculated for each integration using `Eureka!`'s 'mgmc' method. Photometric light

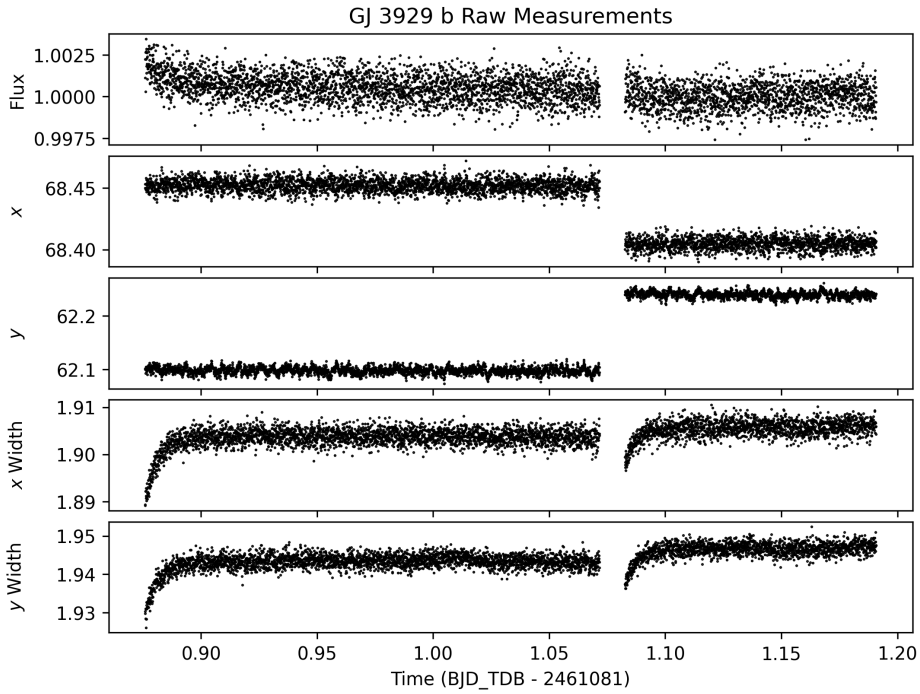

Figure 1: Stability of flux, centroid, and PSF. Time series of changes in the normalized raw flux, centroid position (x, y), and PSF width (computed as a Gaussian standard deviation along the x and y axes), illustrating initial settling behavior, the substantial change in PSF location at the start of Observation 5, and the second-round of settling at the start of Observation 5.

curves were extracted using the `photutils` package with circular apertures and 'exact' edges, where pixels are weighted by the fraction of their area lying within the specified aperture. A range of apertures and background annulus radii were considered, initially. Apertures ranged from 4–11 pixels, in 1-pixels steps. The inner radii of the background annulus varied from 14 to 26 pixels, with Analyst A increasing in 4-pixel steps and Analyst B increasing in 2-pixel steps, while the annulus width ranged from 10 to 30 pixels, with Analyst A increasing in 10-pixel steps and Analyst B increasing in 5-pixel steps.

In Stage 4, we then identified outliers that were 3.5σ discrepant from a box-car median with a 20-integration-wide box. This outlier identification was performed a maximum of 20 times, constructing a mask of all outlier points. A slightly stricter 3.0σ filter was also tested, with no effect on the subsequent results. In the end, we selected the aperture that minimized the median-absolute-deviation for the out-of-eclipse baseline, with both analysts settling on a 5 pixel aperture radius and a background annulus spanning 24 to 54 pixels from the centroid.

3 Light Curve Fitting

Next, we fit the photometric time series in Stage 5. Special attention was spent on identifying and characterizing a proper systematics model due to the nature of the ∼15-minute pause in the observations caused by the visit gap. The effect of the visit gap

can be seen in Figure 1, which shows the position and width of the PSF over time for Observations 4 and 5. A modest ∼30-minute settling ramp occurs at the beginning of Observation 4, after which the centroid is stable until the visit gap. Upon the start of Observation 5, the centroid shifts position by ∼0.15 pixels and another small ∼15-minute settling ramp is seen in the PSF width.

Our light curve model can be summarized as:

$$\mathrm{Model}(t) = E(t) * S(t) + \mathrm{GP}(t),$$

where $E(t)$ is the batman eclipse model and $S(t)$ is the composite systematic noise model. In some fits, we used a Gaussian Process (GP) to further detrend time-dependent systematics, where $\mathrm{GP}(t)$ is the GP predictive model with `celerite2`'s approximation of a Matérn-3/2 kernel as a function of time. We define $S(t)$ as

$$S(t) = P(t)R(t)Y\Big(y(t)\Big)X\Big(x(t)\Big)SY\Big(sy(t)\Big)SX\Big(sx(t)\Big), \tag{1}$$

where

$$P(t) = c_0 + c_1(t - \bar{t})$$

is a linear trend in time where $\bar{t}$ is the mean time,

$$R(t) = 1 + r_0 \exp\Big(-r_1(t - t_{\mathrm{start}})\Big)$$

is an exponential ramp where t_{start} is the time of the first integration. Each of Y, X, SY, SX are linear decorrelation functions defined similarly to each other as

$$Y\Big(y(t)\Big) = 1 + c_y\Big(y(t) - \overline{y}\Big)$$

where $(x(t), y(t))$ is the measured centroid position as a function of time, and $(sx(t), sy(t))$ is the PSF width along the x- and y-axes as a function of time, and $(\overline{x}, \overline{y})$ is the time-averaged centroid position, and $(\overline{sx}, \overline{sy})$ is the time-averaged PSF size. The approximate Matérn-3/2 kernel as a function of time used by our GP is defined as

$$k(t) = \sigma^2 \left[(1 + 1/\epsilon)\ e^{-(1-\epsilon)\sqrt{3}\,t/\rho}\,(1 - 1/\epsilon)\ e^{-(1+\epsilon)\sqrt{3}\,t/\rho}\right],$$

where $\epsilon = 0.1$ and controls the quality of celerite2's approximation of the Matérn-3/2 kernel, ρ controls the length scale of the covariance (and is fitted in `Eureka!` with $m = \ln\rho$), and σ^2 controls the amplitude of the covariance (and is fitted in `Eureka!` with $A = \ln(\sigma^2)$). Lastly, a multiplicative error inflation term is added to the fit to ensure $\chi^2 = 1$ for the best-fits and to address any underestimates in the white noise level from `Eureka!`'s Stages 3–4. All priors for the astrophysical and systematic models are summarized in Table 1.

All fits used the `dynesty` dynamic nested sampling algorithm. Dynamic nested sampling is typically preferred for complex or multi-modal posteriors, as it adaptively allocates live points to focus more efficiently on the regions of interest. It is generally more efficient for parameter estimation, especially when the posterior has sharp features or

multiple peaks. Our sampling began with an initial 512 live points using the 'rwalk' sampling algorithm and the 'multi' bounds and an initial $d \log \mathcal{Z} < 0.01$ stopping criterion (where $\mathcal{Z}$ is the Bayesian evidence). This was then followed-up by iteratively adding batches of 256 live points with a 'pfrac' of 0.9 (favoring a precise posterior distribution over a precise Bayesian evidence) until the default stopping criterion was achieved.

Our primary exploration during light curve fitting was to evaluate what model assumptions and systematics model were appropriate for this dataset. Here, we highlight three areas of investigation: 1) the secondary eclipse time and orbital eccentricity, 2) the treatment of the data around the visit gap, and 3) the inclusion of GPs in the systematics model.

3.1 Results & Discussion

Our initial model consisted of an exoplanet eclipse fixed at the time expected based on a circular orbit and with no GP used in the fit. This initial fit found a very large eclipse depth of 341^{+38}_{-41} ppm for Analyst A and 340^{+40}_{-40} ppm for Analyst B, far larger than the maximum expected eclipse depth of ∼134 ppm for this target assuming zero albedo and zero recirculation (Mansfield et al. 2019). These fits showed only a small amount of residual red noise in RMS versus time bin size plots. By including a GP in the systematics model, Analyst A found a similarly large eclipse with only slightly larger error bars at 305^{+56}_{-50} ppm. Analyst B also experimented with trimming more of the beginning of Observation 4 to avoid the ramp-like settling, finding a similarly large eclipse of 316^{+36}_{-33} ppm.

We next experimented with different assumptions on the eclipse timing. As stated above, our first assumption of a circular orbit results in a deep eclipse occurring directly after the visit gap, at a time when the systematics are still affected by ramps in the PSF behavior (particularly the PSF width). If we leave the time of secondary eclipse completely unconstrained, then Analyst A found a negative eclipse of about 100 ppm is found to start near the end of Observation 5 with the fitted egress occurring after the end of the observations, effectively fitting a step-up in flux for the remainder of the observation.

Because the systematics related to the visit-gap may be biasing the measurement of any eclipse near that time, Analyst A also tested fitting each visit independently, i.e., we fit the data before and after the gap alone. When the data before the gap is discarded, the small ramps at the beginning of Observation 5 can be fit with the exponential ramp parameters of the systematics model. However, this appears to have little affect on the final results, with no eclipse constrained when the eclipse time is freely fit and a deep eclipse found when a circular orbit is assumed (241^{+103}_{-99} ppm with GP). When we discard the data after the visit gap and let the secondary eclipse time vary so that it can occur in Observation 4, we find no evidence of an eclipse.

Lastly, we tested the orbital solution from the RWDDT Core Implementation Team (CIT) JWST Data Analysis Sub-Team's Checkpoint 1 fit that found evidence for a moderate eccentricity (see Table 1). This orbital solution results in an eclipse that begins during the visit-gap and ends approximately 45 minutes into Observation 5. For this fit, Analyst B found an eclipse depth of 125^{+48}_{-47} ppm when fitting both visits. We also discarded the data before the visit-gap and used a GP to model the time-dependent systematics. Here, a somewhat deep eclipse is still found, but with much larger uncertainties (Analyst A:

Table 1: Astrophysical and orbital parameters used in the circular and eccentric orbit fits. Circular orbit parameters are taken from the juliet$_{\rm circ}$ fit from the CIT's orbit fitting efforts during observational scheduling. Eccentric orbit parameters are taken from the CIT's Checkpoint 1 fits that found evidence for moderate eccentricity. Systematic model priors are unchanged between fits. Gaussian priors are shown as $\mathcal{N}(\mu, \sigma)$ with mean μ and standard deviation σ, while Uniform priors are shown as $\mathcal{U}(l, u)$ with lower-limit l and upper-limit u.

Astrophysical model priors		
Parameter	Circular Orbit	Eccentric Orbit
P (days)	2.6162644	2.6162643243
$t_{\rm sec}$ (BJD$_{\rm TDB}$)	$\mathcal{N}(2460765.5434, 0.0015)$	–
t_0 (BJD$_{\rm TDB}$)	–	58955.8965273919
b	0.20	0.5259044225
a/R_*	17.26	17.2974955329
$e\cos\omega$	0.0	-0.0104
$e\sin\omega$	0.0	-0.14
$R_*/R_\odot$[†]	0.315	0.315
$R_{\rm p}/R_*$	0.03045	0.03045
$F_{\rm p}/F_*$ (ppm)	$\mathcal{N}(100, 300)$	$\mathcal{N}(100, 300)$
Systematic model priors		
c_0	$\mathcal{N}(0.999, 0.01)$	
c_1	$\mathcal{N}(0.0, 0.1)$	
r_0	$\mathcal{N}(0.0, 0.01)$	
r_1	$\mathcal{U}(3, 300)$	
c_y	$\mathcal{N}(0.0, 0.5)$	
c_x	$\mathcal{N}(0.0, 0.5)$	
c_{sy}	$\mathcal{N}(0.0, 0.5)$	
c_{sx}	$\mathcal{N}(0.0, 0.5)$	
A	$\mathcal{U}(-24, -10)$	
m	$\mathcal{U}(-7, 0)$	
scatter_mult	$\mathcal{U}(0.8, 10)$	

[†]The stellar radius is used to account for the difference in light travel time throughout the planet's orbit.

191^{+138}_{-129} ppm, Analyst B: 218^{+113}_{-127} ppm), resulting in a statistically insignificant detection of the eclipse. We chose this latter analysis as our fiducial model based on our prior knowledge that the orbital eccentricity may be nonzero and the fact that the eclipse depth is uncertain enough to not be inconsistent with our physical expectation for the maximum eclipse depth of $\sim$134 ppm.

These results overall show evidence for a deep eclipse towards the beginning of the Observation 5, though the timing is poorly constrained and the detection is confounded by ramp-like systematics. In some model fits, including circular-orbit fits with and without GPs, this deep eclipse is unphysically large but statistically significant. On the other hand, eccentric-orbit fits find a somewhat smaller and less significant eclipse. Some of the differences in the statistical significances of the detected eclipse are caused by the visit

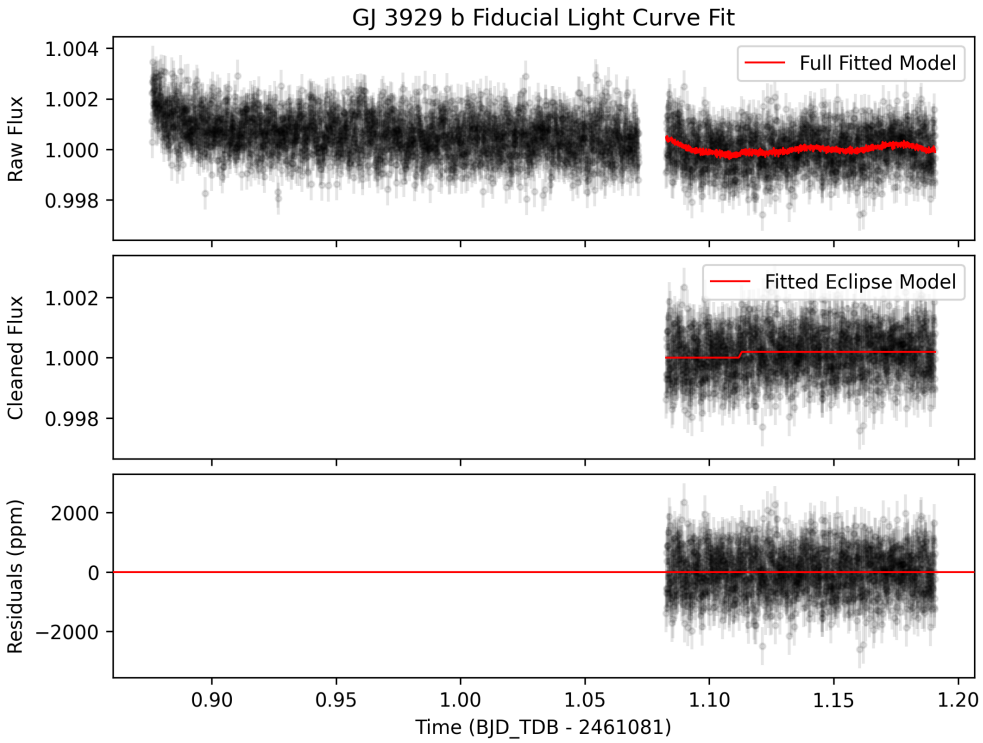

Figure 2: Fiducial light curve fit. *Top:* The raw, normalized flux measurements in black with the (systematic × astrophysical model + GP mean predictive model) over-plotted in red. The first 2980 integrations (i.e., Observation 4) were not included in our fiducial fit. *Middle:* The systematics-divided flux measurements are shown in black, with the fitted eclipse model shown in red. *Bottom:* The "data − model" residuals.

gap, with the eccentric-orbit fits finding an eclipse starting during the visit gap. This results in less observing time during the actual eclipse, coupled with confounding ramp-like systematics occurring *in eclipse*.

Table 2 shows our final fiducial result for the fixed, moderately-eccentric orbit solution with a GP and with the data from Observation 4 discarded. Throughout the fits, the multiplicative error inflation term was found to increase the error to about 750 ppm (20% above photon noise) when GPs were used and to about 780 ppm (25% above photon noise) when GPs were not used.

Table 2: Fiducial eclipse fit results for GJ 3929 b.

	Eclipse Depth [ppm]	$t_{\rm sec}$ [$\rm BJD_{TDB}$]	Residual Std. Dev. [ppm]
Analyst A†	191^{+138}_{-129}	2460765.525986‡	742^{+12}_{-13}
Analyst B	218^{+113}_{-127}	2460765.525986‡	742^{+13}_{-12}

†Our fiducial analysis, whose final and intermediate data products are hosted on MAST as an HLSP.

‡Calculated from the values in Table 1.

4 Calibrated Stellar Flux Measurement

Following the methodology of Gordon et al. (2025), we measured absolutely-calibrated stellar photometry using `calints` FITS files with a 5.69 px aperture and an 8.63–11.45 px background annulus, applying an aperture correction of 1.497. We selected about 3.7 hours of baseline time for the measurement, avoiding the eclipse, beginning-of-visit ramps, and the visit gap. Adding in quadrature the observational scatter with the $\sigma(\mathrm{CF}) = 0.48\%$ and $\sigma(\mathrm{repeat}) = 0.45\%$ terms from Gordon et al. (2025), we obtained a calibrated stellar flux of 18.87 ± 0.12 mJy. As was discussed in the Eclipse 3 report, this is $\sim$10% higher than was found in our original analyses of Eclipses 1–2; the underestimate in the stellar flux from Eclipses 1–2 was caused by an overly aggressive bad-pixel mask in the CRDS reference files used in those analyses, combined with poor quality bi-linear interpolation to replace those marked-bad pixels.

5 Discussion and Outlook

This report provides a **snapshot** from a single eclipse. The eclipse is complicated by a visit gap that takes place near or during the expected time of eclipse. This, combined with the small eclipse signal and systematic noise, results in an inability to robustly constrain the eclipse signal from this single observation. The previous observations from the RW-DDT program can be used to help constrain the eclipse depth and eclipse timing for GJ 3929 b. The CIT's Checkpoint 2 analysis will next simultaneously fit all four eclipse observations which may allow for more robust inferences to be drawn from this fourth dataset. For this particular dataset, care should be taken at the light-curve fitting level to properly account for the ramp-like behavior at the beginning of Observation 5. Overall, given the ramp-like systematics introduced by the visit gap, the loss of continuous temporal coverage associated with that gap, and the fact that orbital parameter uncertainties often mean the eclipse timing is not well known in advance, these results suggest that using multiple exposures per dither is the safer option than splitting observations into multiple linked visits.